UTM Faculty of Mechanical Engineering
UNIVERSITI TEKNOLOGI MALAYSIA
THE ENGINEER STORY

e-ISSN: 3009 - 0792 Volume 20, 2026, 5-9

THE STUDY OF AERODYNAMIC PERFORMANCE THROUGH PASSIVE FLOW CONTROL METHOD IN LOW-SPEED FLOWS

Ahmad Syahin Abu Talib
Faculty of Mechanical Engineering, Universiti Teknologi Malaysia, 81310 UTM Johor Bahru, Johor, Malaysia.
Corresponding author: ahmad.syahin@utm.my

ABSTRACT

This study investigates the effect of micro-ramp passive flow control towards the aerodynamic performance on a NACA 4415 airfoil in low-speed aerodynamics conditions. At higher angles of attack, the baseline airfoil suffers from flow separation driven by a strong adverse pressure gradient on the suction surface. To address this, micro-ramps scaled to 40%, 60%, and 80% of the local boundary layer thickness was modified on the airfoil suction surface. Quantitative measurements were obtained using a three-component force balance. The result shows that improvement of 10% towards the aerodynamic performance using the micro-vortex generators of 60% boundary layer height. These findings suggest that micro-ramps effectively re-energize the boundary layer and delay the flow separation, resulting in a significantly improved lift-to-drag ratio over the baseline NACA 4415 configuration.

KEYWORD

Wind tunnel, micro-ramp, NACA 4415, aerodynamic performance

INTRODUCTION

Flow separation occurs as natural phenomenon in aerodynamics, yet it can have a catastrophic impact on flight efficiency for Unmanned Aerial Vehicles (UAVs) that frequently operate in low-speed, low-Reynolds-number regimes (Yao et al., 2022). Particularly, when the airfoil encounters an adverse pressure gradient, the increasing pressure in the direction of flow decelerates the fluid velocity within the boundary layer, causing flow separation from the surface and resulting in decreased aerodynamic performance (Li et al., 2025). This results in reduction in lift and increased in drag, which directly compromises the endurance and mission profile.

To mitigate these effects, micro-ramp flow control devices are installed on the surface. These devices function as micro-vortex generators, that enables the transfer of energy momentum, from the outer region towards the inner regions of the boundary layer. This helps in delaying flow separation and keeping the downstream flow attached to the surface (Wang et al., 2022). Accordingly, the design selection criteria of the micro-ramp height of 40% to 60% were proven to be effective through an optimization study conducted by Anderson et al. (2006). and later was supported by Saad et al. (2015). in hypersonic flows.

Therefore, to determine the most effective geometry, three configurations were tested in accordance with the δ height of 40% (MR40), 60% (MR60), and 80% (MR80). This is to evaluate the performance of passive micro-ramp flow control on a NACA 4415 asymmetrical airfoil under low-speed operating conditions.

MATERIAL AND METHODOLOGY

The investigation was carried out experimentally using a NACA 4415 airfoil in a subsonic wind tunnel with a velocity, $V = 21$ m/s with a Reynolds number, $Re = 2.0 \times 10^5$. The angle of attack (α) of 0° to 24° with an increment of 2° was conducted throughout the whole test range. All models were fabricated using a 3D printer, an additive manufacturing technology that manufactures parts layer by layer based on CAD designs. Polylactic Acid (PLA) was selected as the material due to its reliability and practicality for prototyping.

The airfoil has a chord length, C = 155 mm and spanwise, S = 250 mm with δ measured at 1.5 mm through particle image velocimetry (Methal et al., 2023). The suction side were modified so that three interchangeable cases of MR40, MR60 to MR80 and a clean surface as the baseline can be tested on the NACA 4415 airfoil. The 40, 60 and 80 after 'MR' case indicates the δ of 80%, 60% and 40% respectively. The position of each micro-ramp was fixed at 0.3 C.

Table 1: Micro-ramp vortex generators parameters of MR40 to MR80 type.

Micro-ramp size	MR80	MR60	MR40
Height, h (mm)	0.96	0.72	0.48
Chord, c (mm)	11.52	8.64	5.76
Width, w (mm)	9.38	7.04	4.68
Spacing, s (mm)	12.00	10.00	4.31

The micro-ramp chord length c , width, w and spacing, s were determined using the optimization conducted by Anderson et al. (2006). All the parameters for the micro-ramp dimensions are listed in Table 1. A detail design of passive micro-ramp flow control slot is shown in Figure 1. The height of micro-ramp in is perpendicular to surface of the slot and the freestream velocity, V is facing upwards.

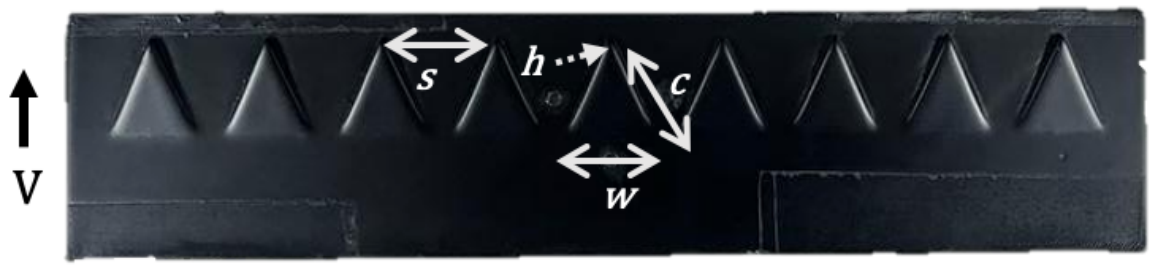

Figure 1: Micro-ramp configuration of height c, chord length c, width w, and spacing s.

Wind Tunnel Facilities

Experiments were conducted at the wind tunnel laboratory at Universiti Pertahanan Nasional Malaysia (UPNM). The wind tunnel model is a Longwin LW-9300R, a suction type mechanism open-loop design. The speed ranges for these experiments were fixed at 21 m/s. A schematic of the wind tunnel is shown in Figure 2. Each test run was recorded and averaged at a sampling time of 20 s with a stable time of 2 s.

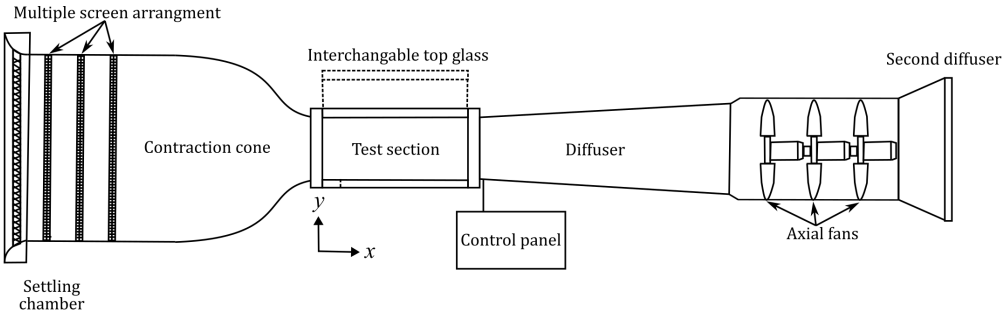

Figure 2: Schematic diagram of a Longwin LW-9300R subsonic wind tunnel.

The test section has a dimension of 0.3 m in height, 0.3 m in width, and 1.0 m in length, with a transparent observation area during testing. Measurements of turbulence intensity showed values ranging from 0.1% to 1.7%, indicating that the wind tunnel operates with very low turbulence levels (Methal et al., 2023).

Experimental Model Arrangement in the Wind Tunnel

A three-component vertical force balance system shown in Figure 3 was used in this study to measure the aerodynamic forces acting on the airfoil model. This type of force balance has an accuracy within a 3% full-scale range and the α can be adjusted to be as low as 0.18° using the side adjustable handle. This force balance is designed so that airfoil model can be mounted vertically in the wind tunnel test section. To attach the airfoil to the force balance, a 6 mm diameter rod was connected through the airfoil while the other end is connected to the force balance system.

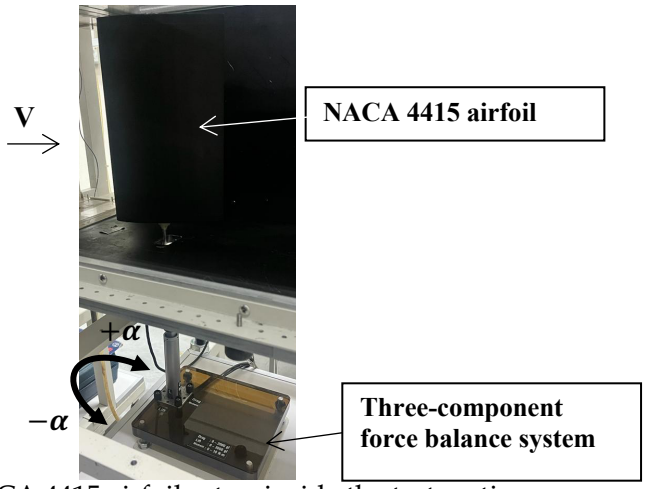

Figure 3: NACA 4415 airfoil setup inside the test section.

RESULT AND DISCUSSION

This study focuses on the aerodynamic performance of different micro-ramp vortex generator on a NACA4415 airfoil. The calculation of the lift coefficient, $C_L$and drag coefficient, C_D accounts for all correction parameters as conducted by Methal et al., 2023. The goal is to identify the best performance for achieving higher C_L and lower C_D. Figure 4 illustrate the relationship between the C_L, C_D and lift-to-drag ratio, C_L/C_D at α 0° to $24^{\circ}$for different MR case.

From the analysis in Figure 4 (a), all the MR case configuration shows a steady and linear increase in C_L as the α increase. A slight improvement can be seen in the case of MR60, where it outperforms the other cases, providing the highest C_L for each α. Conversely, MR40 shows the lowest C_L output before the pre-stall phase ($\alpha = 0^{\circ}$ to 10°) although the margin in comparison with the baseline case becomes smaller and eventually outperforms the baseline case at $\alpha = 14^{\circ}$. The maximum C_L was achieved with the highest peak of 1.1 at $\alpha = 16^{\circ}$ for MR60 case right before the airflow starts to separate significantly from the surface. This is about 16% increase of C_L compared to the baseline case. This is followed by the MR80, which shows an improvement of about 7% relative to the baseline. After reaching the peak, there is a visible drop in C_L indicating the onset stall. The baseline case exhibits a drop after $\alpha = 17^{\circ}$ showing an abrupt stall behaviour. While having a lower initial lift, MR40 demonstrate a stall recovery where C_L begins to increase again and stabilize at high α. This eventually surpasses the C_L of the remaining configurations at a deeper stall regime.

The experimental data suggest that the MR60 is the most effective out of all the cases conducted for enhancing lift during standard flight manoeuvres at low α. However, for higher α and post stall conditions, it is suggested that MR40 offers a better performance by maintaining a more stable characteristics after the initial stall point.

For the drag analysis, Figure 4 (b) represents the C_D versus α. In aerodynamics, drag is the resistive force acting opposite the direction of motion. As shown in Figure 4 (b), the pre-stall phase of ($\alpha = 0^{\circ}$ to 16°) shows an increase in C_D as the α increases. The MR40 shows the least drag penalty and higher drag resistance in comparison to the baseline case at low α with a 20% improvement. In the meantime, MR60 which previously shows the highest C_L, suffers a drag

penalty of 15% increase in C_D over the same range. During drag divergence, a sharp vertical jump can be observed in the curve showing a flow separation. In contrast, the baseline case delays this drag rise with over a longer range, maintaining a lower drag profile at $\alpha = 17^{\circ}$. On another note, MR40 experience a premature drag at $\alpha = 15^{\circ}$, where it nearly doubles than the baseline case. Meanwhile, MR60 and MR80 converge to a similar drag profile at higher α although baseline case remains slightly efficient.

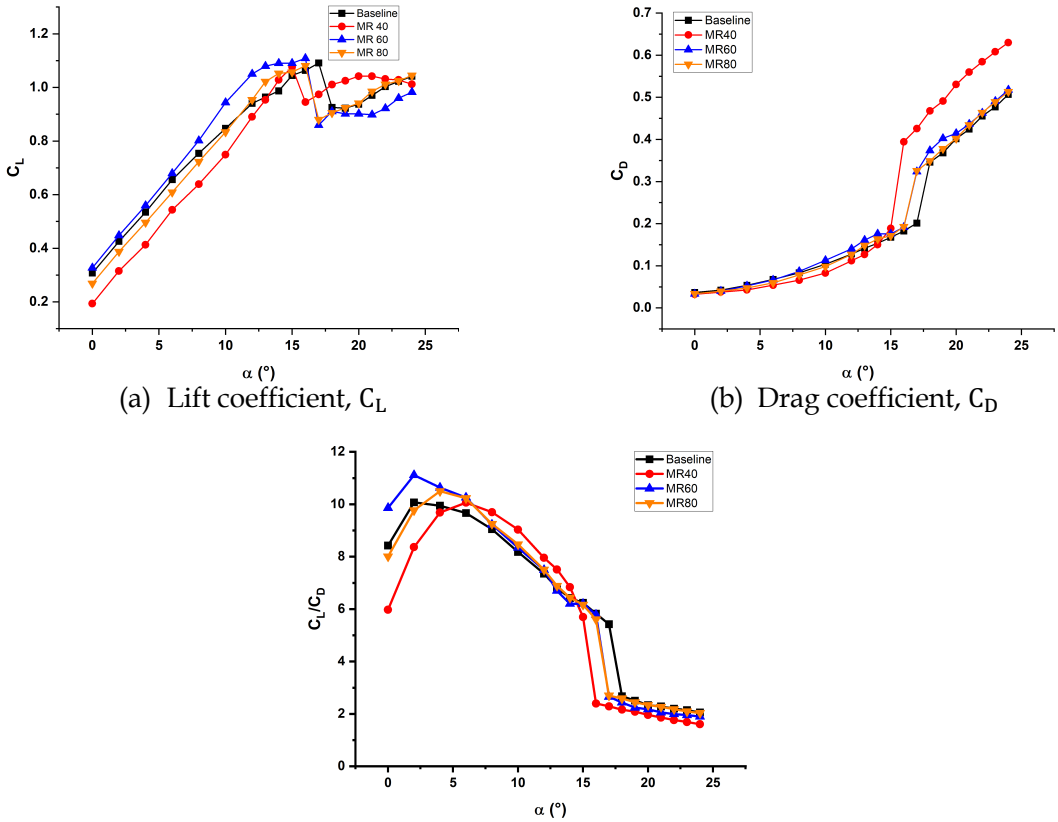

(a) Lift coefficient, C_L (b) Drag coefficient, C_D

(c) Lift-to-drag ratio C_L/C_D

Figure 4: Micro-ramp flow control aerodynamic comparison on NACA 4415 airfoil.

The drag polar analysis reveals a significant trade-off between MR40 and MR60 configurations. While MR60 previously was identified as the most C_L improvement, it incurs a 12% drag penalty during standard operations. In contrast MR40 provides an exceptional 20% drag reduction at moderate α making it efficient in fuel saving providing that it stays below the $\alpha = 15^{\circ}$ threshold.

Figure 4 (c) shows the lift-to-drag ratio C_L/C_D of the baseline and MR cases at $\alpha = 0^{\circ}$ to 24°. This is the most important metric for the aircraft performance as higher value indicates more lift generated over the drag penalty. The maximum efficiency can be seen by the MR60 as it achieves the highest overall efficiency of all the cases, having a peak performance at an $\alpha = 2^{\circ}$.This suggest that MR60 is seen have the most enhanced performance using this micro-vortex generator configuration for cruise and low speed flight regime. However, it must not be forgotten that the MR40 still dominates at higher α than MR60, showing a superior configuration between $\alpha = 7^{\circ}$ to 15°. This indicates that MR40 is effective at maintaining efficiency during high menuevers like ascending and low-speed loitering control. Notably, all configurations show a sharp drop after their respective stall points. This is consistent with the previous graph, as the baseline case

maintains efficiency slightly longer until $\alpha = 17^{\circ}$, whereas the remaining cases drop earlier, at $\alpha = 15^{\circ}$ to 16°.

The analysis of aerodynamic efficiency highlights a clear specialization among the test cases. MR60 provides a 10% increase in efficiency at low α, making it ideal for high-speed cruise conditions. However, as the α increases 10° and above, MR40 emerges as the most efficient configuration, offering an 11% improvement over the baseline. These results suggest that an adaptive MR option of either MR60 and MR40 as the aircraft slows or climbs, could maximize efficiency across the entire flight envelope in certain situations, though care must be taken to manage the slightly earlier stall onset observed in the modified configurations.

CONCLUSION

Based on the analysis, the implementations of micro-ramp modifications significantly alter the airfoil's performance depending on the flight envelope. MR60 shows the highest C_L in low α and linear range, having a 10% over baseline. However, the efficiency drops abruptly after as the α increases, experiencing an abrupt stall. Meanwhile, MR40 has 20% lower C_D at moderate α but higher drag penalty at post-stall.

In overall scenario, the results suggest that an adaptive micro-ramp flow control system for cruise and low-speed flight could yield the most significant aerodynamic benefits. This could provide an enhanced lift-to-drag ratio across the operational range while mitigating the drag penalties observed in standards configurations.

ACKNOWLEDGEMENT

This research was supported by the Ministry of Higher Education (MOHE) through the funding from UPNM/STFC-NEWTON/2018/TK/01. The authors also want to thank Universiti Pertahanan Nasional Malaysia (UPNM) for sponsoring the project through Graduate Research Assistant Fellowship under PPPI Trust Fund UPNM. Special acknowledgement to the staff of Universiti Teknologi Malaysia.

REFERENCE

Anderson, B. H., Tinapple, J., & Surber, L. (2006). Optimal control of shock wave turbulent boundary layer interactions using micro-array actuation. Collection of Technical Papers - 3rd AIAA Flow Control Conference, 2(June), 880–893.

Li, Y., Xue, W., Luo, L., Yan, H., Du, W., & Luo, Q. (2025). Aerodynamic investigation and flow loss control on a newly designed leading-edge fillet in a high-load turbine. Energy, 328, 136617.

Methal, Z., AAT, S. ., MRA, R., & MR, S. (2023). UPNM Subsonic Wind Tunnel Flow Measurements Technique and Calibration: English. PERINTIS eJournal, 13(1), 77–97.

Saad, M. R., Lo, K. H., & Kontis, K. (2015). 29th International Symposium on Shock Waves 2. 29th International Symposium on Shock Waves 2, November 2016, 1–7.

Wang, Z., Chang, J., Kong, C., Huang, R., & Xin, X. (2022). Experimental investigation of micro-ramp control for shock train under various incoming flow conditions. Physical Review Fluids, 7.

Yao, Y., Ma, D., Zhang, L., Yang, X., & Yu, Y. (2022). Aerodynamic Optimization and Analysis of Low Reynolds Number Propeller with Gurney Flap for Ultra-High-Altitude Unmanned Aerial Vehicle. Applied Sciences, 12(6), 3195.